Journal of Molecular Liquids 313 (2020) 113451

Contents lists available at ScienceDirect

Journal of Molecular Liquids

journal homepage: www.elsevier.com/locate/molliq

Interaction of doxorubicin hydrochloride in the presence of, mixed aggregate of ibuprofen sodium and cationic lipid

Guanyi Li [a], Anirudh Srivastava [b,*], Chenyu Liu [a], Weihong Qiao [a,*]

[a] State Key Laboratory of Fine Chemicals, School of Chemical Engineering, Dalian University of Technology, Dalian 116024, PR China
[b] Central Research and Incubation Center, Department of Chemistry, Swami Vivekan and Subharti University, Subhartipuram, NH-58, Delhi-Haridwar Bypass Road, Meerut 250005, Uttar Pradesh, India

ARTICLE INFO

Article history:
Received 25 February 2020
Received in revised form 24 May 2020
Accepted 26 May 2020
Available online 06 June 2020

Keywords:
Lipid
Mixed aggregate
Binding constant
Encapsulation
Controlled drug release
Cytotoxicity

ABSTRACT

This research was highlighted the importance of mixed aggregates based on drug-lipid to improve the interaction of one or more drugs in aqueous medium. This mixed aggregate can significantly inhibit the growth of MCF-7 cells, and has great potential for anti-inflammatory and cancer treatment after tumor removal. The cationic lipid (CL) has been synthesized with multistep reaction and is characterized by ^{1}H NMR and mass spectroscopy. CL and ibuprofen (IBF) physiochemical analysis was investigated using surface tension, conductance, dynamic light scattering (DLS), and electron microscope transmission (TEM). The strong synergism between mixed aggregate (LIB) system CL and IBF was observed. The study on UV spectroscopy measured that the LIB mixed aggregate showed optimum binding to doxorubicin hydrochloride (DOX) and the binding constant *Log* K_b was 6.17 compared to single CL, the *Log* K_b was 5.83. Binding results indicated that the DOX was more encapsulated in mixed LIB aggregates compared to single CL aggregates. This mixed aggregate LIB has excellent performance in controlling the release of drugs. For single CL aggregate, approximately 62.5% DOX was released after 72 h (pH = 7.4). However, LIB such as, $(0.1\alpha_{CL} + 0.9\alpha_{IBF})$, the release of DOX decreased to 16.08%. Finally, LIB mixed aggregate applicability has been used to minimize the cytotoxicity of MCF-7 cells, and it has been found that DOX in LIB mixed aggregates has a higher inhibitory effect on cell growth than DOX in CL.

1. Introduction

In recent years, drugs have evolved towards the multi-agent delivery system, such as drug-amphiphilic mixed aggregates, which is a clinically common procedure for treating malignant diseases and has significantly improved survival and quality of life due to the potential for additive or synergistic effects [1,2].The multi-agent delivery system, which includes multiple agents with specific therapeutic effects or biological functions, has been gaining growing interest in recent years because of its advantages in combination therapies [3–6] or in tissue regeneration and engineering. For example, the mixed aggregate of diphenhydramine hydrochloride and anionic sodium deoxycholate (SDC) and non-ionic transglycosylated stevia (Stevia-G) surfactants was developed by our group researcher Srivastava et al. to increase the encapsulation performance of ethenzamide. In this study, they prepared mixed aggregate using mole fraction formulation that could control the excess drugs and surfactants that could lead to high encapsulation of drugs and high cellular uptakes [7]. Zheng et al. have prepared mixed anticancer drug doxorubicin (DOX)-loaded inorganic rod-like nano-hydroxyapatite (n-HA) particles in poly (lactic-*co*-glycolic acid) (PLGA) by the electrospun hybrid nanofibers [8]. Recent studies demonstrated the multi-drug loading and the temporally programmable release of each drug have become essential criteria in cancer therapy [9,10]. Yang et al. proposed the fabrication of hydrophobic curcumin encapsulated micelles assembled from biodegradable poly(ethylene glycol)-polycaprolactone copolymer and hydrophilic DOX in the polyvinyl alcohol solution, followed by simple electrospinning this combination. They studied a time-programmed release of hydrophilic DOX (short-term) and hydrophobic curcumin (long-term) [11]. However, the short-lived DOX released lasted only for 10 days whereas the long-term curcumin released lasted for as short as 30 days, which was insufficient for long-term tumor healing. It is considered a significant challenge to achieve controlled the release of multi-drug with distinct properties in a sequential as well as a sustained manner and few studies were reported on this aspect [12–14].

As we all know, ibuprofen is a child antipyretic and anti-inflammatory drug jointly recommended by the World Health Organization and the US FDA. It has anti-inflammatory, analgesic, and antipyretic effects, but it can stimulate the digestive system, nervous system, and kidneys. Therefore, the study of ibuprofen sustained-release agents

* Corresponding authors.
E-mail addresses: ani_srivastava83@yahoo.co.in (A. Srivastava), qiaoweihong@dlut.edu.cn (W. Qiao).

https://doi.org/10.1016/j.molliq.2020.113451
0167-7322/

is favored by many researchers. Zhao et al. [15] developed a new strategy for the self-coated interfacial layer on drug-loaded mesoporous silica nanoparticles (MSNs) based on mussel-mimetic catecholamine polymer (polydopamine, PDA) layer between inorganic and organic matrix for controlling drug release. When the interface PDA was coated and MSNs encapsulated in electrospun poly(L-lactide) (PLLA) fibers, the release rates of drugs located inside/outside the interfacial layer could be finely controlled. The short-term anti-inflammation Ibuprofen (IBF) could release for 30 days in the absence of interfacial interactions and sustained long-term doxorubicin (DOX) could release for 90 days in the presence of interfacial interactions, which was helpful to inhibit potential tumor recurrence. Cole and Pierce et al. [16,17] explained the way of long-term anti-cancer drug delivery along with short-term anti-inflammatory drug release inhibited a tumor reappearance after surgery and the tumor resection site. In this system, the anti-inflammatory drug may decrease the risk of inflammation and cancer recurrence by inhibiting inflammatory cell growth, and the anticancer drug destroys the tumor cells. Moreover, biodegradable scaffolds provide a suitable microenvironment for healthy cell growth and so support tissue regeneration. These studies showed how important the multi-agents delivery system was for drug delivery.

This study was aimed to establish a versatile and general methodology for improving the efficiency of the delivery system. We have developed a novel nano-sized multidrug delivery system based on drug-surfactant interaction. The physicochemical interaction between the drug molecule and the surfactant system significantly improves the solubility of the drug, avoids the drug from forming a precipitate in the solution during the injection process, and reduces side effects [18,19]. Considering the physio-chemical interactions between drugs and surfactants, the appearance of surfactants may increase the absorption of drugs. Therefore, a systematic study was proposed to describe the interactions of drugs with a variety of surfactants.

Mixed aggregates with high encapsulating efficiency and controlled release have received much attention for the drug delivery system [20]. In this work we have used Gemini cationic lipids (CL), which have low cmc and are increasingly reported as multipurpose materials like gene therapy [21–25] and drug encapsulation [26–30], capturing the interest of the scientific communities. Due to the size, biocompatibility, and protective effect of CLs on the degradation of encapsulating substances, CLs are suitable for the administration of drugs and diagnostic agents regardless of the route taken (oral, injectable, parenteral or lung). Our previous studies described the efficiency of CL encapsulated DNA for gene delivery [21]. The variable length of carbon chains and the quaternary ammonium or neutral tertiary amine heads of CL allowed us to find the structure-function relationship of how these factors affect cationic lipids on gene delivery performance. CL gene vectors in the condition of carbamate as connection bond and hydroxyalkyl group as a head group may improve the gene therapy transfection efficiency and lower cytotoxicity [24].

In the current system, Ibuprofen (IBF) and doxorubicin (DOX) are used, in which the former contains a carboxylic group and hydrophobic moiety, and the latter contains liposoluble anthraquinone ligand, phenolic hydroxyl, and basic amino groups. It used as a clinically common combination drug in tumor treatment which could offer the advantages of increasing the tumoricidal efficacy and reducing the side effects caused by the high-dose of a single medication. The IBF and DOX were expected to bind into the inner core through ionic interaction and hydrophobic effect [31].

In this work, we have prepared mixed aggregates of CL and IBF using mole fraction based formulation ($C^*(\alpha_{CL} + \alpha_{IBF})$). The physicochemical properties of CL-IBF mixed aggregate were determined using surface tension and conductance experiments methods. The interaction parameter and thermodynamic interfacial parameters was evaluated by Clint's, Rubingh, and Motumura's equations. The applicability of prepared mixed aggregate was used to enhance the binding properties and encapsulation of DOX. After encapsulating DOX, the slow-release effect of these aggregates on DOX was examined by dialysis experiments. Finally, the cytotoxicity of mixed aggregates on MCF-7 cell lines was tested to verify the application effect of the prepared aggregate which simultaneously encapsulate two different drugs and have a sustained release function. The structure of CL and IBF was shown in Fig. 1(A & B).

2. Experimental

Materials and Methods was representing in the electronic supportive information (ESI) from 2.1 to 2.6 sections.

2.7. Synthesis of cationic lipid (CL), 2,3-bis(dodecyloxy)-N-ethyl-N,N-dimethylpropane-1-aminium chloride

2.7.1. Synthesis of 1-dimethylamino-2,3-propanediol

70.9 g (520 mmol L^{-1}) of a 33% dimethylamine aqueous solution was added and stirred in a 250 mL three-necked flask. Weigh 6 g of sodium hydroxide and arranged it as a 40% aqueous solution. When it was cooled to room temperature, add it into a three-necked bottle. 44 g (400 mmol L^{-1}) of 1-chloro-2,3-propanediol was weigh into a dropping funnel and added slowly into the bottle. In the three-necked bottle, the control acceleration was 1–2 drops/s. After the addition was completed, the reaction was performed at 30 °C for 24 h. Then a distillation apparatus was installed, and the temperature was gradually increased to 105 °C to distill off the excess dimethylamine. After distillation, the distillation apparatus was removed, and the three bottles were heated and stirred opened until the evolved gas had no amine taste. The water was removed under reduced pressure, and after completion, the fraction of 102–104 °C/2 mmHg was collected by distillation under reduced pressure. 60% yield was observed. The reaction scheme was shown in the Fig. 2(1).

2.7.2. Synthesis of dodecyl p-toluenesulfonate

124.9 mmol L^{-1} of lauryl alcohol and 39.5 g of pyridine were added to a 250 mL three-necked bottle, and the flask was immersed in an ice-water bath to make the temperature of the mixture 0 °C. 26.25 g (138.1 mmol L^{-1}) of p-toluenesulfonyl chloride are added to the bottle in portions within 20–30 min at this temperature. The mixture was stirred for 12 h under 20 °C. and diluted with a solution of 100 mL of hydrochloric acid (specific gravity 1.19) and 300 mL of ice water. The crystallized ester was filtered through a chilled Buchner funnel and blotted as dry as possible. The solid was transferred to a 500 mL beaker, and add 100 mL of methanol, then the mixture was heated in a water bath until the ester melted. It was cooled in an ice-water bath with constant stirring, and the ester precipitated very finely. It is filtered on a frozen funnel and dried in air (preferably below 20 °C). The crude product was recrystallized from petroleum ether (30–60 °C) and the solution was cooled to 0 °C. The resulting ester was filtered through a frozen funnel to give the product. 70–80% yield was observed. The reaction scheme was shown in the Fig. 2(2).

2.7.3. Synthesis of N, N-dimethyl-dodecyloxypropylamine

N,N-dimethylaminopropylene(*2.4 g*, *20 mmol*), p-toluenesulfonate (60 mmolL^{-1}), potassium tert-butoxide (6.72 g), and xylene were added to a 100 mL single-mouth flask equipped with a reflux condenser and a three-way charge/discharge valve. After pumping vacuum with a

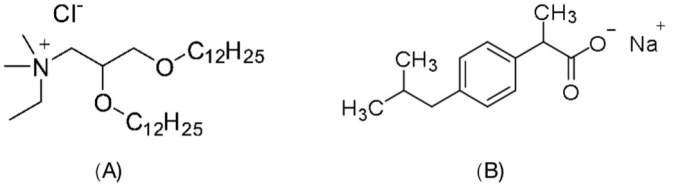

Fig. 1. (A) The structure of 2,3-bis(dodecyloxy)-N-ethyl-*N*,*N*-dimethylpropane-1-aminium chloride(*CL*)and (B) Ibuprofen sodium salt.

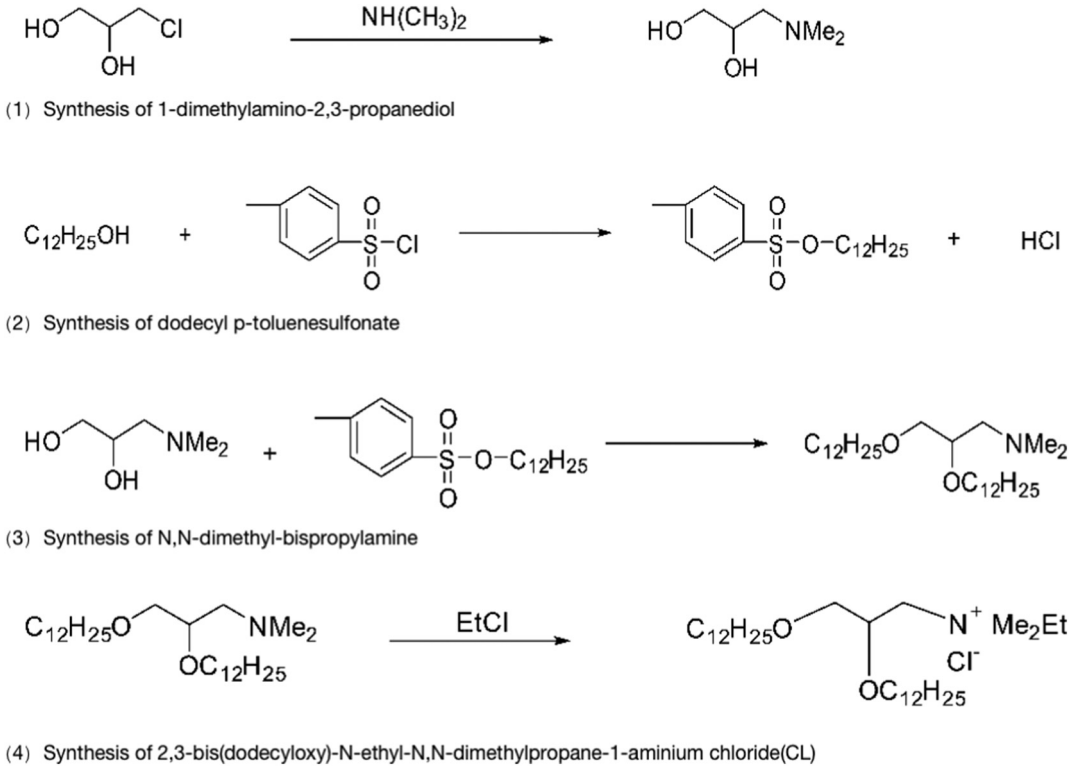

Fig. 2. Representation of multistep reaction of cationic lipid.

water pump and filling with nitrogen, the mixture was heated to 140 °C, and refluxed for 3 h. After cooled, it was washed with water, and the organic phase was dried over anhydrous Na_2SO_4 and the solvent was distilled off under reduced pressure. The concentrate was chromatographed on silica gel using petroleum ether/ethyl acetate (2:1) as eluent to get the product. 20% yield was observed. The chemical reaction scheme was shown in the Fig. 2(3).

2.7.4. Synthesis of target molecule

The appropriate *N*, *N*-dimethyl-bisalkoxypropylamine and 60 equivalents of the appropriate ethyl chloride were added to the autoclave, respectively. The autoclave reacted at 70 °C for 48 h. After the reaction was completed, the autoclave was cooled to 0 °C, and the lid was opened in a fume hood to allow the excess halogenated hydrocarbons to be volatilized (chloromethane and ethyl chloride), or filtered by adding 30 mL of petroleum ether to the autoclave (for iodine methane, iodoethane) giving a crude product. The crude product was recrystallized in petroleum ether or acetonitrile to obtain the target product. 95% yield was obtained. The reaction was shown in the Fig. 2(4) [32,33]. CL ^{1}H NMR was shown in Fig. S1 and data was shown as below:

CL: ^{1}H NMR (400 M, $CDCl_3$) δ 4.10 (m, 1H, O*CH*), 3.91 (s, 2H, NCH_2), 3.68–3.44 (8H, NCH_2CH_3, $CHCH_2O$, 2 × OCH_2), 3.33 (s, 6H, N(CH_3)$_2$), 1.55 (s, 2 × OCH_2CH_2), 1.41 (s, 3H, NCH_2CH_3), 1.26 (s, 36H, 18 × CH_2), 0.88 (s, 6H, 2 × CH_2CH_3); HRMS *m/z*: Found $[M - Cl]^+$ 484.5092, $C_{31}H_{66}ClNO_2$ calcd. for $[M - Cl]^+$ 484.5094.

3. Results and discussion

3.1. Critical aggregation concentration of IBF-CL

The *cac* values of pure IBF, CL and LIB at different mole fractions of IBF (α_{IBF}) were obtained from the representative plots of specific conductance (κ)and surface tension (γ) measurements, shown in Fig. S2 and Fig. 3. The mixture consisted of cationic and anionic amphiphiles. The strong coulombic interaction shows that the *cac* of the mixed systems is surprisingly lower compared to the possible ideal mixture, and this type of mixture is called catanionic system. In a 25 °C aqueous solution, the *cac* value of IBF reached 179.5 mmolL^{-1}, which was close to the literature value [34–36]. The *cac* value of pure CL reached 0.0025 mmolL^{-1} (Table 1 and Fig. 3). As shown in Fig. 1(B) that the IBF molecule was small hydrophobic part and, as a result, forming associates at upper concentrations in comparison to usual surfactant with α_{IBF} increase. The presence of two hydrophobic tails makes CL more hydrophobic, shown in Fig. 1(A). Therefore, their *cac* values are extremely low compared to conventional cationic surfactants [35].

In the LIB mixtures, *cac* increases in aqueous solution with increasing mole fraction (α_{IBF}). This suggests a strong synergistic interaction between IBF and CL, since this promotes more hydrophobicity around CL in the mixture, thereby ensuring that aggregation starts to occur at lower concentrations than pure CL amphiphiles (Table 1). Table 1 and Fig. 3 showed that the *cac* value of CL was much lower than that of the IBF *cac*; thus, CL would immediately form micelles and drug molecules would intercalate into CL micelles. Cationic lipid molecules are more effective in reducing the *cac* of the mixed LIB system, as the two hydrophobic chains of cationic lipid enhance the hydrophobic interaction between IBF and CL molecules.

3.2. Interaction parameters for IBF- CL mixed aggregate

The values of *cac* of the mixed LIB (*cac**) were determined from the relationship between *cac** and the *cac's* of IBF (cac_1) and CL (cac_2) and the form was Eq. (1):

$$\frac{1}{cac^*} = \frac{\alpha_1}{cac_1} + \frac{(1-\alpha_1)}{cac_2} \quad (1)$$

In Eq. (1) α_1 refers to the mole fraction of the IBF or CL in the bulk medium, *cac** is the *cac* of the mixed micelle when it was assumed to behave ideally according to the Clint's equation [7,37]. The *cac* values of the mixed amphiphiles calculated according to the Clint's equation were termed as ideal *cac* values (*cac**), as shown in Table 1 and also in Fig. S3. From Fig. S3 it was apparent that the experimental values of

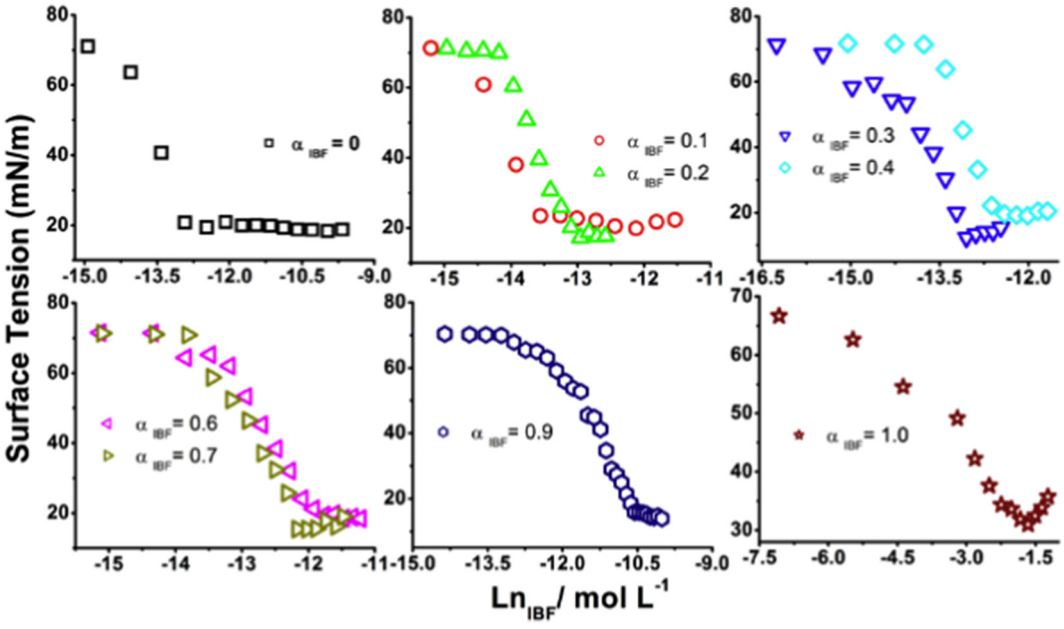

Fig. 3. Representative surface tension (γ) plots of LIB mixtures vs. Ln_{IBF}/mol L^{-1} in the aqueous medium at 25 °C.

cac were slightly smaller than the ideal values, which indicates that the LIB system has a synergistic effect in aqueous media.

In order to estimate the molar fraction of the drug in the mixed aggregate, the conventional solution theory of Rubingh [7,37–39] is used, and the equation gives the value of the molar fraction (X_1) of the first component using Eq. (2),

$$\frac{X_1^2 \ln(\alpha_1 cac/X_1 cac_1)}{(1-X_1)^2 \ln[(1-\alpha_1)cac/(1-X_1)cac_1]} = 1 \quad (2)$$

where *cac* was the LIB mixed systems and X_1 was the mole fraction of the drug IBF in the mixed micelle.

For all mixed systems, the micelle mole fraction X_1 increases slightly with the increase in IBF mole fraction. The mole fraction of the drug in the ideal state (X^{id}) is calculated using the Motumura's approximation [40–44] in Eq. (3).

$$X^{id} = \left[\frac{(\alpha_1 cac_2)}{(\alpha_1 cac_2 + (1-\alpha_1)cac_1)}\right] \quad (3)$$

Fig. 4 illustrates a comparison of X_1 (Rubingh's) and X^{id} (Motomura's) as a function of the mole fraction of a drug. Fig. 4 shows that the X_1 values of all studied mixed systems (CL) are higher than their respective X^{id} values over the entire mole fraction range. These results indicate that the mixed micelle phase is rich in IBF molecules. The change in X_1 observed from the X^{id} value indicates that all the mixed systems deviate from the ideal behavior.

Eq. (2) was solved to obtain the values of X_1 (Table 1) which was used for the calculation of the interaction parameter, β_m by Eq. (4),

Table 1
Experimental cac^{ex} and ideal cac^* (mmolL^{-1}), micellar compositions of IBF (X_1), ideal micellar compositions of IBF (X_1^{id}), interaction parameter (β_m), activity coefficients (f_1,f_2,f_1 refers to IBF, f_2 refers to CL), excess free energy (ΔG^o_{ex}, kjmol^{-1}) and surface excess (Γ,10^{-6} mol m^{-2}) of mixed micellization for LIB mixtures in aqueous medium at 25 °C.

α_{IBF}	cac^*	cac^{ex}	X_1	X_1^{id}	β_m	f_1	f_2	ΔG^o_{ex}	Γ
0	0.0025	0.0025	/	/	/	/	/	/	7.726
0.1	0.0027	0.0013	0.177	0.823	−18.31	0.000004	0.568	−6.590	7.253
0.2	0.0031	0.002	0.141	0.859	−14.97	0.000015	0.745	−4.487	9.322
0.3	0.0035	0.0022	0.149	0.851	−14.64	0.000024	0.723	−4.596	8.657
0.4	0.0041	0.0033	0.103	0.897	−11.86	0.000075	0.882	−2.712	8.596
0.6	0.0062	0.0055	0.073	0.926	−9.654	0.000251	0.949	−1.625	6.866
0.7	0.0083	0.0052	0.155	0.844	−12.54	0.000131	0.739	−4.080	5.246
0.9	0.0249	0.022	0.078	0.922	−7.715	0.001418	0.954	−1.373	5.733
1	179.5	179.5	/	/	/	/	/	/	2.190

Standard uncertainties (u) were u(T) = ±0.2 °C. Relative standard uncertainties, u_r for $cac = \pm 5\%$, u_r for $(X_1/X^{id}) = \pm 5\%$, u_r for $(\beta_m) = \pm 5\%$, u_r for $(f_1, f_2) = \pm 5\%$, u_r for $\Delta G^o_{ex} = 5\%$ and u_r for $\Gamma = 5\%$.

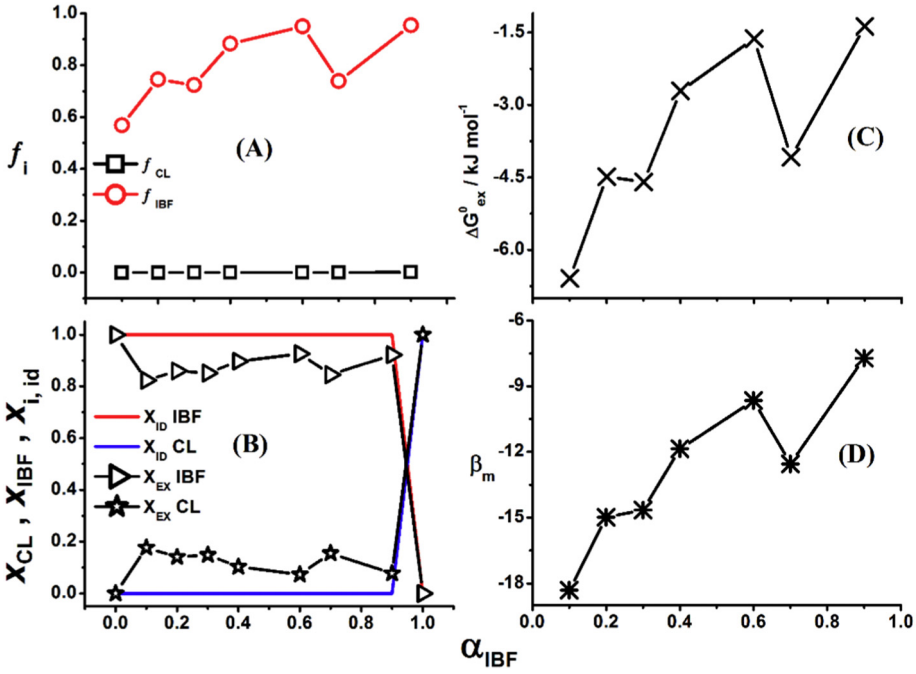

Fig. 4. Experimental values of (A) activity coefficients (f_1,f_2), (B) micellar compositions (X_1), ideal micellar compositions (X_1^{id}), (C) excess free energy (ΔG^o_{ex}) and (D) interaction parameter (β_m) of mixed micellization for LIB mixtures in aqueous medium at 25 °C.

$$\beta_m = \frac{\ln\left(\frac{cmc\alpha_1}{cmc_1 X_1}\right)}{(1-X_1)^2} \tag{4}$$

β_m values give the information on both the nature and strength of the interaction between LIB mixed aggregates. According to Rubingh [38,39], an attractive interaction or synergism in the mixed systems was represented with a negative β_m. Two conditions must be followed for mixed aggregates formation: 1) Interaction parameter β_m must be negative, and (2) $\beta_m > ln(cac_1/cac_2)$ [40]. LIB mixed systems followed above both the conditions, which represented the non-ideality of the LIB system. All the systems were showed strong synergism with the -β_m average values, ($-\beta_m$ avg) for IBF as −12.81 with CL respectively shown in Fig. 4 and listed in Table 1. This more attractive interaction of CL favours the aggregation due to the presence of two hydrophobic tails which increases their hydrophobicity. The non-ideal behavior of the mixed systems was evaluated by following Eqs. (5) and (6) to give the activity coefficients (f_1,f_2) values [38,39]:

$$f_1 = exp\left[\beta.(1-X_1)^2\right] \tag{5}$$

$$f_2 = exp\left[\beta.(X_1)^2\right] \tag{6}$$

f_1 and f_2 of all mixed systems were found to be less than unity and f_1 for IBF was lower than f_2 for CL which confirmed the participation of CL in mixed micelles, shown in Fig. 4 and Table 1.

3.3. Thermodynamics of micellar and interfacial behavior

The counter ion binding constant β_c was calculated from the relation [41] $\beta_c = S_2/S_1$, where S_1 and S_2 are the slopes of the relationship curve between the conductivity and the concentration below and above the *cac*(Fig. S2), respectively and the values of β_c obtained were shown in Fig. 6 and Table 2. The β_c values of mixed aggregates were controlled entirely by the CL, in the stern layer of the mixed aggregates, heads of CL were probably more exposed than those of IBF. Gibb's free energy of micellization (ΔG^o_m) [42] was calculated using Eq. (7) and the values were presented in Fig. S4 and the values were also listed in Table 2:

$$\Delta G^o_m = RT\left[(1+\beta_c)\ \ln cac + X_1\ \ \ln\alpha_1 + X_2\ \ln\alpha_2\right] \tag{7}$$

The negative values of ΔG^o_m revealed that the entire LIB mixed aggregate systems have the considerable spontaneity of aggregation.

The excess free energy of micellization, ΔG^o_{ex}, could be evaluated by using the following Eq. (8)

$$\Delta G^0_{ex} = [X_1.\ \ln f_1 + (1-X_1).\ \ln f_2].RT \tag{8}$$

The mixed studied system of IBF, CL, ΔG^o_{ex} shown in Fig. 4, values were negative, and their magnitude decreased with an increase in mole fraction of IBF, which indicates that the large number of IBF molecules introduced makes the mixed aggregates have a more stable interaction.

CL is adsorbed at the air-solution interface and reduces the γ of the solution. Generally, the maximum surface excess (Γ) represents the amount of CL adsorbed at the air-solution interfacial surface, shown in Fig. S5. Based on the Gibbs adsorption isotherm applied in the case of a single ionic surfactant, and the adsorption layer is electrically neutral, the formula for surface excess (Γ) is:

$$\Gamma = -[1/(2RT)](d\gamma/dlnc_s) \tag{9}$$

Γ was either Γ_{CL} or Γ_{IBF} depending upon whether the solution was a CL or IBF. The values of $d\gamma/dlnc_s$ for CL and IBF were obtained by data fitting and by substituting these values in Eq. (9). We found that the average value of Γ_{CL} for CL was 7.72×10^{-6} mol m^{-2}and Γ_{IBF} for IBF was 2.19×10^{-6} mol m^{-2}, respectively.

The values of Γ_{IBF} at each *cac* agree well with literature values [35,36]. In order to determine the surface excess value in the mixture of IBF and CL, we adopted the method of Rosen and Hua [43]. In this way, we used the Eqs. (10) and (11) between the activities.

$$\beta_a = \ln f_{1a}/x_{2a}{}^2 = \ln f_{2a}/x_{1a}{}^2 \tag{10}$$

Table 2
Values of the bulk concentration $C_{m\gamma}$ (mmol L^{-1}), monolayer composition (x_{1a}), monolayer activity coefficients (f_{IBF},f_{CL}), binding constant (β_c), interaction parameter (β_a) and Gibb's free energy of micellization, kjmol^{-1}(ΔG_m^o) in the monolayer corresponding to the surface tension of 40 mN m^{-1} (±0.5).

α_{IBF}	$C_{m\gamma}^{id}$	$C_{m\gamma}{}^{ex}$	x_{1a}	x_{1a}^{id}	β_a	β_c	f_{CL}	f_{IBF}	ΔG_m^o
0.0	0.0015	0.0015	/	/	/	0.3864	/	/	/
0.1	0.0016	0.0009	0.8375	0.1625	−16.61	0.3604	0.000008	0.6447	−45.68
0.2	0.0018	0.0012	0.8670	0.1330	−13.85	0.4665	0.000029	0.7812	−47.68
0.3	0.0021	0.0011	0.8355	0.1645	−14.72	0.4534	0.000034	0.6702	−46.91
0.4	0.0024	0.0022	0.9280	0.0720	−9.941	0.4489	0.000191	0.9482	−45.31
0.6	0.0037	0.0030	0.8960	0.1040	−10.23	0.4285	0.000270	0.8928	−42.86
0.7	0.0049	0.0038	0.8840	0.1160	−10.13	0.3810	0.000363	0.8710	−41.63
0.9	0.0149	0.0131	0.9176	0.0824	−7.246	0.3218	0.002239	0.9517	−35.12
1.0	63.900	63.900	/	/	/	0.2859	/	/	/

Standard uncertainties (u) were u(T) = ±0.2 °C. Relative standard uncertainties, u_r for $C_{m\gamma}$ = ±5%, u_r for ($x_{1a}/x_{1a}{}^{id}$) = ±5%, u_r for (β_c), u_r for β_a = ±5%, u_r for ($f_{IBF}f_{CL}$) = ±5% and u_r for ΔG_m^o = 5%.

$$x_{1a}{}^2 \ln\left[\alpha_1 c_{m\gamma}/(x_{1a}c_{1\gamma})\right] = (1-x_{1a})^2 \ln\left[(1-\alpha_1)c_{m\gamma}/\{(1-x_{1a})c_{2\gamma}\}\right] \quad (11)$$

In the above Eq. (11), $c_{1\gamma}$, $c_{2\gamma}$ and $c_{m\gamma}$ were the bulk concentrations of CL, IBF and LIB ($\alpha_{1CL} + \alpha_{2IBF}$ mixture), respectively, at the chosen value of constant surface tension, γ = 40 mN m^{-1}. The interaction parameter β_a from Eq. (10) reflects the extent of interaction between the IBF and CL in the adsorbed layer. Eqs. (10) and (11) were analogous to Eqs. (6) and (4). The computed values of $c_{1\gamma}$, $c_{2\gamma}$,$c_{m\gamma}$, f_{1a}, f_{2a} and β_a were shown in Fig. S4 and Table 2. Through using Ghosh and Moulik [44] to treat mixed amphiphiles and combining isotherms of Gibbs adsorption, we could obtain the current mixture equation.

$$d\gamma = -RT\,(\Gamma_{CL} + \Gamma_{IBF} + \Gamma_C)\,dlnc_s = -RT\Gamma_{total}dlnc_s \quad (12)$$

where Γ_{CL}, Γ_{IBF} and Γ_C represent for the surface excess of CL, IBF and the counterions, respectively. In writing Eq. (12), the activity terms were considered to be approximately equal to the corresponding concentration terms. In the counterions sodium (from IBF) and chloride (from CL), the one which could bind to the adsorption layer will depend upon whether $\Gamma_{CL} > \Gamma_{IBF}$ or $\Gamma_{CL} < \Gamma_{IBF}$. Since $x_{1a}/x_{2a} = \Gamma_{CL}/\Gamma_{IBF}$, we got a relation for Γ_{total} as.

$$\Gamma_{total} = \Gamma_{CL} + \Gamma_{IBF} + \Gamma_C = \Gamma_{CL}(1/x_{1a}) + \Gamma_C \quad (13)$$

If we considered the adsorption layer containing CL and IBF to be electrically neutral, then Eq. (13) could be written as $\Gamma_{total} = (2/x_{1a})\Gamma_{CL}$. Therefore, Γ_{CL} or Γ_{IBF} could be computed from the Eq. (14)

$$d\gamma = -RT\Gamma_{CL}\,(2/x_{1a})dlnc_s = -RT\Gamma_{IBF}\,(2/x_{2a})dlnc_s \quad (14)$$

We determined $d\gamma/dlnc_s$ at $c_{1\gamma}$, $c_{2\gamma}$and $c_{m\gamma}$ by fitting the γ versus lnc_s data to polynomials [45] and then computed the values of Γ_{CL} and Γ_{IBF} at the reference point of γ = 40 mN m^{-1}, which was shown in Fig. S5 and Table 1. Γ_i increased as the concentration of all mixtures LIB increased. The adsorption of CL on the adsorption layer is larger than that of IBF, which may reduce the repulsive force of the IBF head group, so that there may be more molecules CL presence on the interface.

3.4. Binding behavior of IBF in CL, DOX in CL and DOX in mixed LIB

The UV absorbance of IBF and DOX in solutions as a function of the concentration of vesicles was used to evaluate the binding constants of IBF in CL, DOX in CL and DOX in mixed LIB complexes, shown in Fig. 5. We were prepared 0.01 mmol L^{-1} stock solutions of CL, IBF and DOX in aqueous medium. For IBF in CL and DOX in CL binding study, IBF and DOX was kept constant 0.02 mmol $L^{-1}$and varying concentration of CL from 0.016 to 0.083 mmol L^{-1}. Similarly, DOX in mixed LIB, DOX concentration 0.02 mmol $L^{-1}$was kept constant in the LIB solutions with varying α_{IBF} concentration from 0.016 to 0.083 mmol L^{-1}.

The measurement has performed the absorbance at a wavelength of 260 and 480 ± 2 nm for IBF and DOX (Fig. 5). The following equation was used to fit the experimental data to obtain binding constant K_b [46,47].

$$\frac{1}{A-A_w} = \frac{1}{A_m-A_w} + \left(\frac{1}{K_b(A_m-A_w)}\right)\left(\frac{1}{(c-c_0)}\right)^{N_m} \quad (15)$$

where A was the measured absorbance, A_w was the absorbance of IBF/DOX in the absence of CL, A_m was the absorbance of IBF/DOX bound to CL, c_0 was the cmc of CL, c is the concentration of CL, N_m was the moles of IBF/DOX-binding micelle per mole, and K_b was the binding constant. The plots of $1/(A - A_w)$ versus $1/(c - c_0)$ were shown in Fig. 5(D–F), and their linearity indicated the applicability of Eq. (15) when N_m was 1.0. The binding constant K_b was calculated from the slope and intercept ratio.

The UV–visible measurements signified the formation of 1:1 or (0.5 + 0.5):1 mixed complexes between IBF, DOX, DOX in LIB, the complexation equilibria. N_m of 1.0 for drugs–aggregate binding was introduced in Eq. (15). The K_b of IBF in CL was log ($K_{IBF\text{-}CL}$) = 5.22 ± 0.2 for present study. Jin et al. [48] was determined the binding constant *log* ($K_{IBF\text{-}HSA}$) = 4.45 of S-ibuprofen in the presence of human serum albumin (HSA). Mahajan et al. [36] explained the molecular interactions of IBF with a surface active ionic liquid (IL), 1-dodecyl-3-methylimidazolium chloride (C_{12}mimCl). They determined the binding constant was log ($K_{IBF\text{-}C12mimCl}$) = 3.19. Also, they explained the formation of highly surface active catanionic complexes (C_{12}mim + IBF) of 1:1 stoichiometry stabilized largely by a combination of electrostatic and hydrophobic interaction due to long alkyl chain length. Similar observation was found in the present IBF in CL system, shown in Fig. 5D.

For DOX in CL system, the K_b value of DOX was found *log* ($K_{DOX\text{-}CL}$) = 5.83 ± 0.2, shown in Fig. 5 E. Similar binding behavior was observed for DOX in dimyristoylphosphatidylcholine (DMPC) and dipalmitoylphosphatidylcholine (DPPC) vesicles by Burke et al. [49]. They were shown that structural changes in both the aglycon and

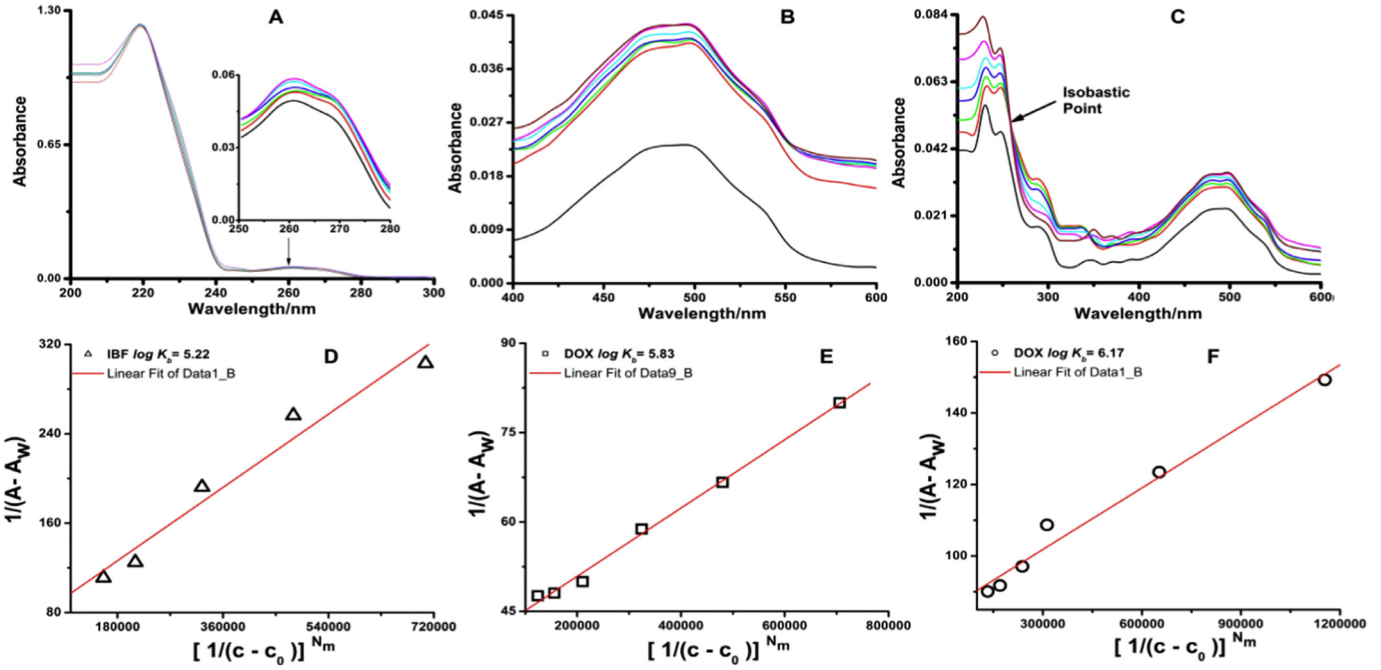

Fig. 5. Representative UV spectra. (A) UV Spectra of IBF (0.02 mmol L^{-1}) in CL, (B) UV Spectra of DOX (0.02 mmol L^{-1}) in CL and (C) UV Spectra of DOX (0.02 mmol L^{-1}) in IBF in CL mixture with varying concentration. Plots (E, D & F) according to Eq. (15) showing the variation of $1/(A - A_w)$ with $[1/(c - c_0)]^{Nm}$ at different concentration. For (A), CL (mmol L^{-1}) were (1) 0.0, (2) 0.016, (3) 0.023, (4) 0.04, (5) 0.05 and (6) 0.066, respectively. For (B & C), CL and α_{IBF} concentration (mmol L^{-1}) were (1) 0.0, (2) 0.016, (3) 0.023, (4) 0.04, (5) 0.05 (6) 0.066 and (7) 0.083, respectively.

amino sugar portions of the drugs molecules strongly modulated binding values for DMPC and DPPC bilayers. They were determined the association constant $log\ (K_{app}) = 5.64$ for DMPC and DPPC vesicles. For DOX in LIB system, the K_b value of DOX was found $log(K_{(DOX)} = 6.17 \pm 0.2$, shown in Fig. 5F. This system was shown high DOX K_b value as compared to single CL systems. From Fig. 5(A & C), DOX in the presence of LIB system showed an interesting outcome. IBF (260 nm) and DOX (480 nm) were spectral overlap at 222 nm from Fig. 5(A & C) and no new peak arising in the spectrum. Interesting from Fig. 5C was also shown an isobastic point at 260 nm of DOX in LIB mixture. This observation was indicated of equilibrium or strong binding of DOX in LIB mixed aggregate medium. An intensities increase was observed for DOX with increase concentration of α_{IBF} 0.016 mM to 0.083 mmol L^{-1}in the mixture at the wavelength 480nmfrom Fig. 5C, which indicated intermolecular interaction between the IBF and DOX [7].

3.5. Investigation on the morphology and size of aggregates

The hydrodynamic diameters of the aggregates formed by the LIB mixtures were determined by the DLS and TEM measurements and were shown in Fig. 6.

For the IBF aggregate, the value of size was found to be 193.0 nm, which was in good agreement with the reported values by Mahajan et al. [36]. The value of size of CL aggregate was found to be 132.9 nm. The size values of mixed aggregate of $\alpha_{IBF} = 0.1$, 0.3, 0.6, 0.7 and 0.9 were found to be 175.1, 117.6. 82.53 and 74.32 nm, respectively. The size of aggregates in the region of $\alpha_{IBF} = 0.9$ high values 133.7 nm and that at $\alpha_{IBF} = 1.0$ was equal to132.9 nm, shown in Fig. 6G. The TEM image of the LIB mixture of $\alpha_{IBF} = 0.1$, 0.6 and 0.9 was also shown in Fig. 6(A–C) and the size of the aggregates estimated from these images were comparable to the size value obtained from the DLS. The shapes of the aggregates in $\alpha_{IBF} = 0.1$, 0.3, 0.6, and 0.9 mixture seem to be irregular, prolate ellipsoidal and branched shaped [50–53], shown in Fig. 6 (A–C). From the DLS and TEM data it may be concluded that large aggregate structures were formed at $\alpha_{IBF} = 0.1$ to 0.9.

It was interesting that when 0.25 mM DOX added into LIB mixture $\alpha_{IBF} = 0.1$, 0.6 and 0.9 and shape of aggregates were change to spherical to tubes or rod-like structure, shown in Fig. 6(D–E). The possible reason was for structure changes that at α_{IBF} 0.9 the amount of IBF was more than α_{CL} and when DOX added, it was strongly bound with IBF as explained in Section 3.3, which increased the electrostatic interaction between IBF and DOX.

3.6. Zeta potential of the LIB mixed aggregates

Measurements of the zeta potential were commonly used to assess the stability of the colloidal system [54]. Generally, when the absolute zeta potential value is <30 mV, the particles tend to aggregate and flocculate [55]. Instead, due to the strong electrostatic repulsion between the particles, they could exist stable for a long time by stopping the process of gather-together and flocculation. Fig. 6H showed the relationship between the zeta potential and α_{IBF}. The total concentration (C) of LIB was controlled at 0.5 mmol L^{-1} as α_{IBF} was from 0.1 to 0.9, which was larger than the *cac* values determined above. Zeta potential measurements were indicated the changes in the surface charge density of IBF or CL mixed aggregates, which could evaluate the stability of colloid suspensions. The region between α_{IBF} 0.7–1.0 in Fig. 6H was the thermodynamic instability region with zeta potential between −30 mV and + 30 mV. It was clearly seen in Fig. 6H that the charge density on the aggregates was decreased with the increasing of α_{IBF} from 0.1 to 0.9. It could be possible that when α_{IBF} is increased, the number of lamellae in multilayer bilayer vesicles was increased as more Na^+ brought into the bilayer, leading to a decreased in zeta potential. It was shown that, after added 0.25 mmol $L^{-1}$of DOX into LIB mixture with varying α_{IBF} from 0.1 to 0.9, the stability of aggregates was slightly changed but highly stable for α_{IBF} 0.9 system.

3.7. In-vitro release study

In vitro DOX and IBF entrapment efficiency (EE%) and controlled release (%) abilities were studied in different aggregate solutions. In this study we prepared IBF in CL, DOX in CL, and DOX in LIB mixed aggregate solution. It was the first time to propose that different types of drugs (such as DOX) be encapsulated by the drug-CL mixture, and the drug-

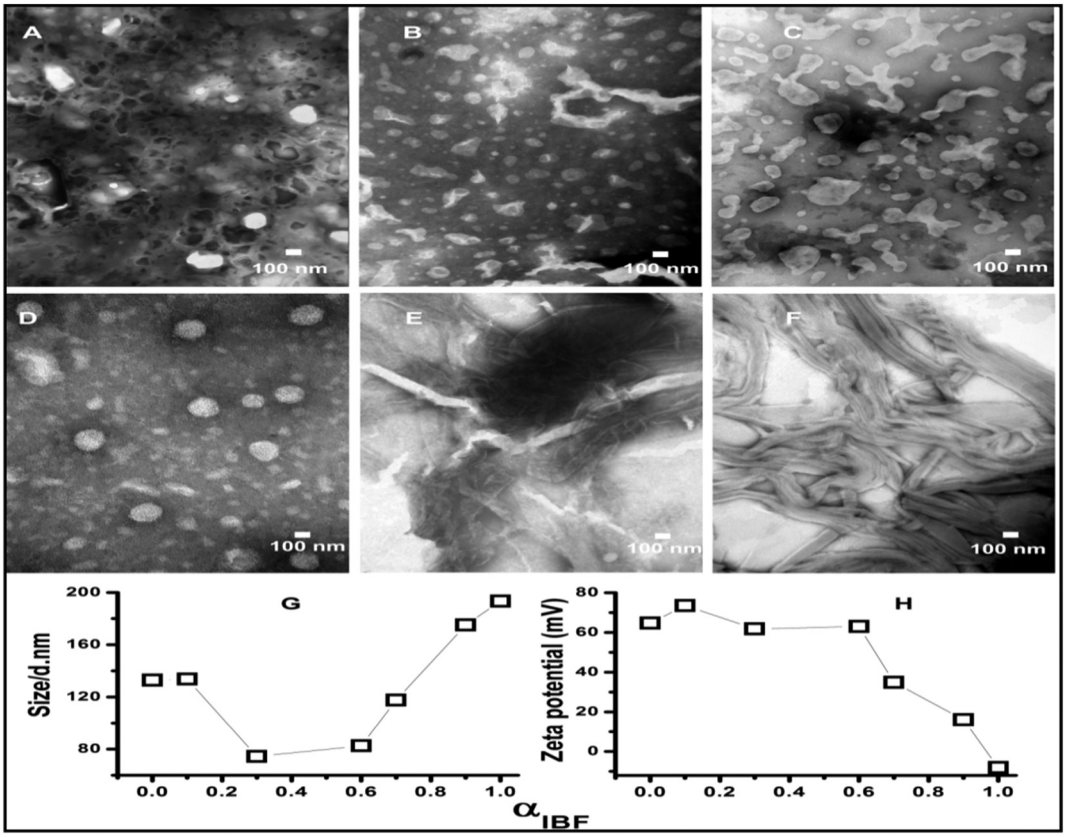

Fig. 6. Typical TEM images A = $\alpha_{IBF}0.1 + \alpha_{CL}0.9$, B = $\alpha_{IBF}0.6 + \alpha_{CL}0.4$ and C = $\alpha_{IBF}0.9 + \alpha_{CL}0.1$. D = ($\alpha_{IBF}0.1 + \alpha_{CL}0.9$) + DOX, E = ($\alpha_{IBF}0.6 + \alpha_{CL}0.4$) + DOX and F = ($\alpha_{IBF}0.1 + \alpha_{CL}0.9$) + DOX, here DOX 0.25 mmol L^{-1}. Variation in size (D_h) (E) and Zeta potential (F) of (□) for CL with α_{IBF}.

CL mixture itself would release the drug (such as IBF) in the same solution. All the solution was prepared in PBS pH 7.4.

EE was determined in 0.5 mmol L^{-1} of CL and 0.25 mM of both drugs IBF and DOX in dialysis method. For DOX in the presence of LIB mixture, we studied EE at α_{IBF} 0.1, 0.6 and 0.9. FL measurement was used to determine the entrapped drug amounts into aggregates, shown in Table 3. The Table 3 and Fig. 7 could show that DOX (68.21%) was more encapsulated than IBF (32.31%) due to hydrophobic interaction with CL. The FL wavelength was shifted from lower to higher wavelength after dialysis; red shift indicated the strong interaction between drug and CL. The possible explanation was that DOX was aggregate about 0.841 mmol L^{-1} [56] and IBF was 179 mmol L^{-1} [34–36]. Due to the fast aggregation cause more EE in DOX in CL solution than IBF in CL solution, which enhanced the DOX interaction with hydrophobic tail of CL surfactant. It was become more effective EE for DOX when DOX was added into LIB mixture. The EE was increased as compared to DOX in CL solution, shown in Fig. 7 and Table 3.

As shown in Fig. 8 and Table 3, from DLS, it could be seen that the size before dialysis was lower and after dialysis was higher. The value of zeta potential was changed from 30 to 68 mV, shown in Table 3, which indicated that the stable aggregate was formed for DOX in LIB. Before dialysis, as the TEM images shown in Fig. 6(D, E, and F), the shape of vesicles changed from spherical to tubular or rod-like structures, when α_{IBF} at 0.1, 0.6, and 0.9, indicating a strong interaction between IBF and DOX. Especially when α_{IBF} was 0.9 and DOX was 0.25 mM, the tubes or rods like structure were found, shown in Section 3.4 and Fig. 6F.

In vitro release was studied using dialysis methods for 72 h in PBS pH 7.4. The free IBF and DOX were released about 90% after 10 h, respectively. The characterization of DOX and IBF release was explored with the combined IBF in CL, DOX in CL and DOX in LIB for better understanding the drug release and multidrug release behavior with different formulations at 37 °C, shown in Fig. 9 and Table 4. For IBF, the controlled release from IBF in CL was slower than free IBF, followed by a sustained release for 72 h, shown in Fig. 9. IBF release from DOX in LIB mixed aggregates was much slower with α_{IBF} increasing, shown in Fig. 9 and Table 4. It indicated that about 49% IBF released from ($0.1\alpha_{CL} + 0.9\alpha_{IBF}$) + DOX aggregates after 72 h at pH 7.4, where about 77% IBF release from IBF in CL aggregates. For DOX, the controlled release from DOX in LIB was much lower than DOX in CL and free DOX, respectively. It was indicated that about 16.08% DOX was released from ($0.1\alpha_{CL} + 0.9\alpha_{IBF}$) + DOX aggregates, where about 61% DOX release from DOX in CL aggregates. The reason of a slower release of DOX than IBF was stronger electrostatic interaction between IBF and DOX with $\alpha_{IBF} > 0.6$, as Section 3.3 explained the binding behavior of DOX in the presence of IBF and CL. This delay in drug release was indicated their potential as a drug carrier, which could minimize the exposure to healthy tissues while increasing the accumulation of therapeutic drugs in specific parts of the body [31].

Table 3
Characterization of aggregates before (BD) and after dialysis (AD) for 7 h, and EE% after 7 h.

Sample at pH 7.4	Average size/nm		Zeta potential/mV		PDI	EE/%
	BD	AD	BD	AD		
DOX in CL	155	192	12.2	29.3	0.525	68.21
IBF in CL	194	257	50.2	30.1	0.485	32.31
($0.9\alpha_{CL} + 0.1\alpha_{IBF}$) + DOX	122	378	52.0	68.0	0.521	86.36
($0.4\alpha_{CL} + 0.6\alpha_{IBF}$) + DOX	126	154	46.6	32.0	0.525	81.37
($0.1\alpha_{CL} + 0.9\alpha_{IBF}$) + DOX	120	140	40.4	30.0	0.453	76.07

Standard uncertainties (u) were u(T) = ± 0.2 °C. Relative standard uncertainties, u_r for size = ±5%, u_r for zeta potential = ±5%, u_r for PDI = ±5% and u_r for EE% = ±5%.

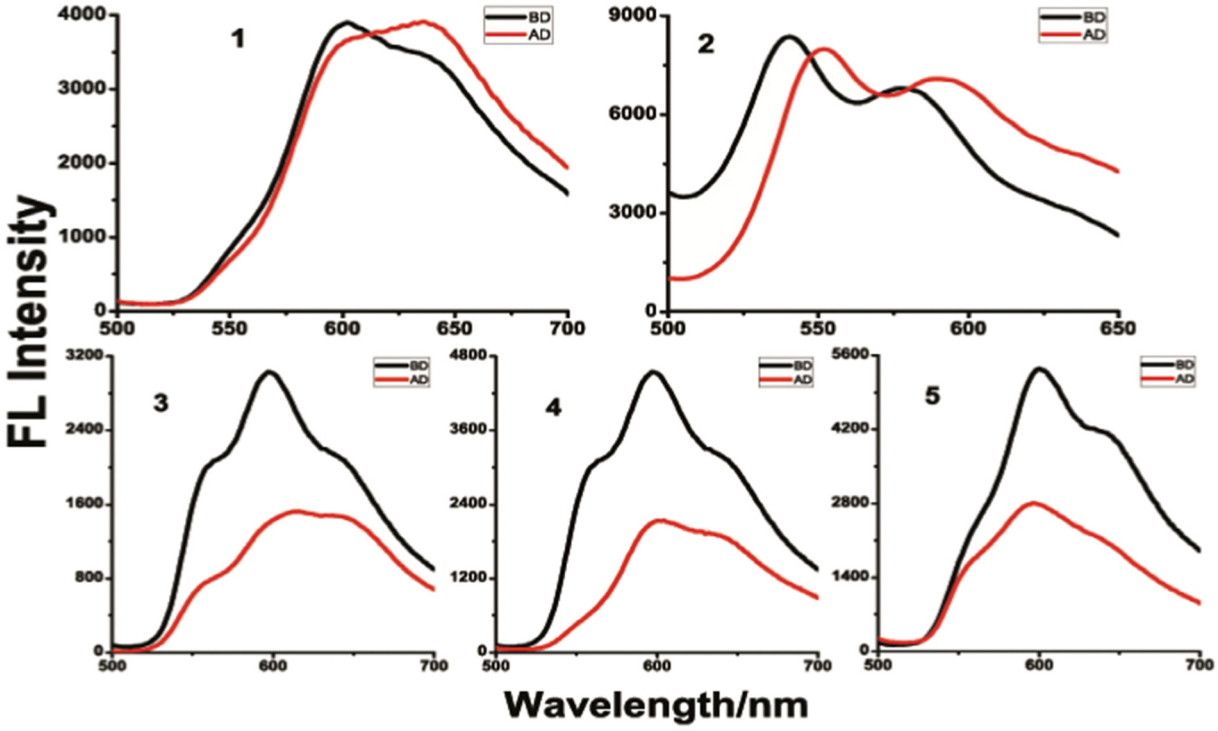

Fig. 7. The plots of FL intensity vs wavelength/nm for (1) free DOX (2) free IBF, (3, 4 & 5) DOX from α_{IBF} 0.1, 0.6 & 0.9.

3.8. Cytotoxicity

To verify the pharmacological activity and biocompatibility, IBF, DOX, CL and DOX in LIB were in-vitro studied on MCF-7 cell lines over 72 h, shown in Fig. 10.

The cell viability of MCF-7 cell lines was studied in the presence of only IBF, DOX and CL from 20 to 100 μmol L^{-1}, respectively, shown in Fig. 10(A). The cytotoxicity of IBF, DOX, and CL was >85% at 40 μmol L^{-1}. The cytotoxicity studies of IBF in CL and DOX in CL were indicated that the cell viability of IBF in CL mixture was 90% and DOX in CL was 46.56% at 40 μmolL^{-1}, shown in Fig. 10(B). At 40 μmol L^{-1}, the cell viability was not much affected by CL, IBF and LIB, which indicated the good biocompatibility. From Fig. 10(C), the cell viability of DOX in LIB was gradually decreased from 60.04 to 31.01% as α_{IBF} was from 0.1 to 0.9. The cell viability of DOX in LIB was lower than DOX in CL, which was possibly because (1) the enhanced permeation and retention (EPR) [57–59] effect was to improve the accumulation of mixed aggregate in cancer cells and (2) the strong binding of DOX with LIB mixture

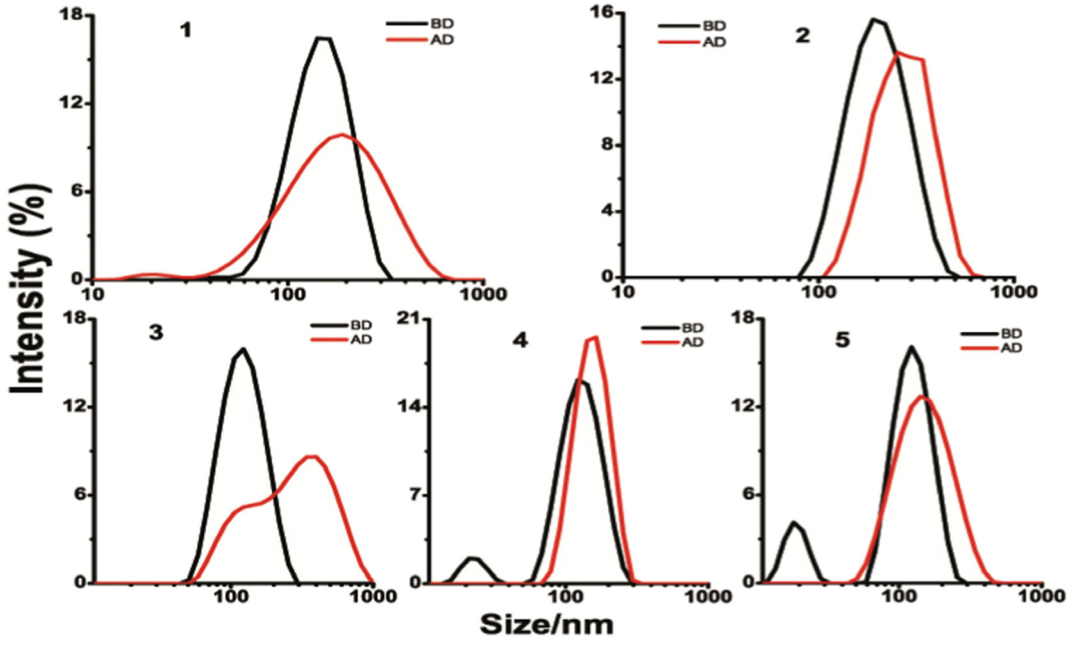

Fig. 8. The plots of size variation using dialysis for (1) free DOX (2) free IBF, (3, 4 & 5) DOX from α_{IBF} 0.1, 0.6 & 0.9.

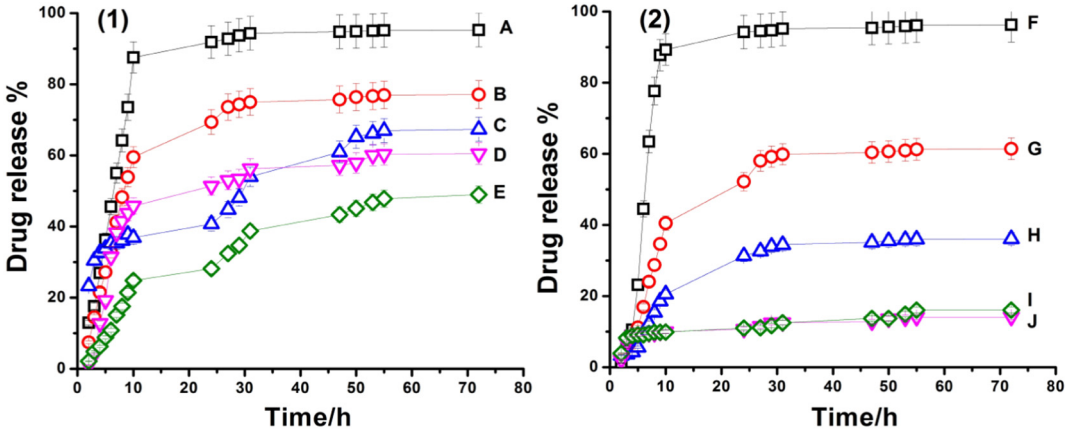

Fig. 9. The profiles of in-vitro release vs time (1) IBF release from (A) free IBF, (B) IBF in CL, (C, D & E) at α_{IBF} 0.1, 0.6 & 0.9, and (2) DOX from (F) free DOX, (G) DOX in CL, (H, I & J) DOX in LIB at α_{IBF} 0.1, 0.6 & 0.9 in PBS (pH 7.4) at 37 °C.

Table 4
In-vitro release of DOX and IBF at pH 7.4 after 72 h.

Samples	DOX release/%	IBF release/%
Free DOX	95.16	–
Free IBF	–	96.06
CL + DOX	61.25	–
CL + IBF	–	77.13
$(0.9\alpha_{CL} + 0.1\alpha_{IBF})$ *+ DOX*	36.04	67.23
$(0.4\alpha_{CL} + 0.6\alpha_{IBF})$ *+ DOX*	14.24	60.54
$(0.1\alpha_{CL} + 0.9\alpha_{IBF})$ *+ DOX*	16.08	49.00

was observed (Fig. 5(C)) which caused the apparent inhibition of the proliferation ability of cancer cells. The critical point of current study was that the formulation based on mole fraction could reduce the toxicity of high concentrations of DOX. The above results indicate that aggregates enhance the absorption of DOX by MCF-7 cells, which has great potential for anti-inflammatory and cancer treatment after tumor removal.

4. Conclusions

The synergistic and hydrophobic interaction was found between IBF and CL. TEM, DLS and Zeta potential results indicated the formation of multi shape(spherical, rod-like or tubular) aggregates. Due to electrostatic interaction and hydrophobic interaction, the binding capacity of DOX and LIB is greater than that of IBF and CL. The in-vitro release experiments represented the release efficiency of DOX from mixed aggregates formulation, which was effectively demonstrated that the mixed aggregates were the controlled the release rate of DOX. Cytotoxicity experiments was evaluated that DOX in LIB systems entered MCF-7 cancer cells mainly by endocytosis and could accelerate the remarkable DOX accumulation in tumor cells. It was indicated that DOX in LIB mixed aggregates have obvious inhibitory effect on the growth of MCF-7 cells. The present study provides an alternative formulation to enhance the interaction between two drugs in the mixed aggregate system. Finally, the drug-lipids mixed aggregated system has great potential applications in the fields of controlled release and multidrug delivery to cure diseases.

Credit authorship contribution statement

Guanyi Li: Investigation, Methodology, Data curation. **Anirudh Srivastava:** Conceptualization, Data curation, Writing - original draft. **Chenyu Liu:** Writing - review & editing. **Weihong Qiao:** Conceptualization, Funding acquisition, Writing - review & editing.

Declaration of competing interest

We declare that we have no financial and personal relationships with other people or organizations that can inappropriately influence our work, there is no professional or other personal interest of any nature or kind in any product, service and/or company that could be construed as influencing the position presented in, or the review of, the manuscript entitled, “Interaction of doxorubicin hydrochloride in the presence of mixed aggregate of ibuprofen sodium and cationic lipid”.

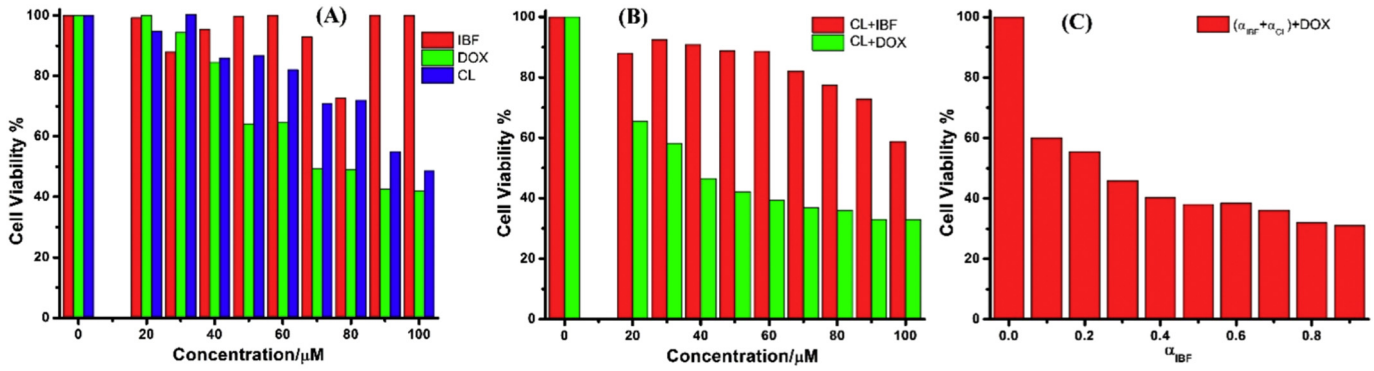

Fig. 10. In-vitro cytotoxicity of (A) free IBF, DOX & CL, (B) IBF in CL &DOX in CL, and (C) DOX in LIB aggregates against MCF-7 cell lines, after 24 h incubation respectively.

Acknowledgements

The research was supported by International Science and Technology Cooperation Program of China No. 2015DFA41670 and the Fundamental Research Funds for the Central Universities DUT19GJ203.

Appendix A. Supplementary data

Supplementary data to this article can be found online at https://doi.org/10.1016/j.molliq.2020.113451.

References

[1] D. Finzi, J. Blankson, J.D. Siliciano, J.B. Margolick, K. Chadwick, T. Pierson, K. Smith, J. Lisziewicz, F. Lori, C. Flexner, T.C. Quinn, R.E. Chaisson, E. Rosenberg, B. Walker, S. Gange, J. Gallant, R.F. Siliciano, Latent infection of CD4+ TCells provides a mechanism for lifelong persistence of HIV-1, even in patients on effective combination therapy, Nat. Med. 5 (1999) 512–517.
[2] T.P. Richardson, M.C. Peters, A.B. Ennett, D.J. Mooney, Polymeric system for dual growth factor delivery, Nat. Biotechnol. 19 (2001) 1029–1034.
[3] B.A. Luxon, M. Grace, D. Brassard, R. Bordens, Pegylated interferons for the treatment of chronic hepatitis C infection, Clin. Ther. 24 (2002) 1363–1383.
[4] O.F. Bathe, S. Ernst, F.R. Sutherland, E. Dixon, C. Butts, D. Bigam, D. Holland, G.A. Porter, J. Koppel, S. Dowden, A phase II experience with neoadjuvantirinotecan (CPT- 11), 5-fluorouracil (5-FU) and leucovorin (LV) for colorectal liver metastases, BMC Cancer 9 (2009) 156.
[5] Y. Kakeji, E. Oki, A. Egashira, N. Sadanaga, I. Takahashi, M. Morita, Y. Emi, Y. Maehara, Phase II study of biweekly docetaxel and S-1 combination therapy for advanced or recurrent gastric cancer, Oncology 77 (2009) 49–52.
[6] H.B. Fung, E.A. Stone, F.J. Piacenti, Tenofovir disoproxil fumarate: a nucleotide reverse transcriptase inhibitor for the treatment of HIV infection, Clin. Ther. 24 (2002) 1515–1548.
[7] A. Srivastava, H. Uchiyama, Y. Wada, Y. Hatanaka, Y. Shirakawa, K. Kadota, Y. Tozuka, Mixed micelles of the antihistaminic cationic drug diphenhydramine hydrochloride with anionic and non ionic surfactants show improved solubility, drug release and cytotoxicity of ethenzamide, J. Mol. Liq. 277 (2019) 349–359.
[8] F. Zheng, S. Wang, M. Shen, M. Zhu, X. Shi, Antitumor efficacy of doxorubicin-loaded electrospunano-hydroxyapatite–poly (lactic-co-glycolic acid) composite nanofibers, Polym. Chem. 4 (2013) 933–941.
[9] E. Jo, S. Lee, K.T. Kim, Y.S. Won, H.S. Kim, E.C. Cho, U. Jeong, Core-sheath nanofibers containing colloidal arrays in the core for programmable multi-agent delivery, Adv. Mater. 21 (2009) 968–972.
[10] X. Xu, X. Chen, Z. Wang, X. Jing, Ultrafine PEG-PLA fibers loaded with both paclitaxel and doxorubicin hydrochloride and their in vitro cytotoxicity, Eur. J.Pharm. Biopharm. 72 (2009) 18–25.
[11] G. Yang, J. Wang, L. Li, S. Ding, S. Zhou, Electrospun micelles/drug-loaded nanofibers for time-programmed multi-agent release, Macromol. Biosci. 14 (2014) 965–976.
[12] B. Zhou, C. Wu, J. Chang, Dual drug release from electrospun poly (lactic-co-glycolic acid)/Mesoporous silica nanoparticles composite Mats with distinct release profiles, ActaBiomater 8 (2012) 1901–1907.
[13] B. Song, C. Wu, J. Chang, Controllable delivery of hydrophilic and hydrophobic drugs from electrospun poly (lactic-co-glycolic acid)/mesoporous silica nanoparticles composite mats, J Biomed Mater Res B Appl Biomater 100 (2012) 2178–2186.
[14] M. Chen, X. Zhu, D. Yan, Sequential drug release for synergistic Cancer treatment and immunity promotion, RSC Adv. 3 (2013) 13399–13405.
[15] X. Zhao, J. Jingwen, Z.Y. (William) Lin, G. Pan, Y. Zhu, Y. Cheng, W. Cui, Self-coated interfacial layer at organic/inorganic phase for temporally controlling dual-drug delivery from electrospun fibers, Colloids Surf. B 130 (2015) 1–9.
[16] W. Coles, Cole chronic inflammation and breast cancer recurrence, J. Clin. Oncol. 27 (2009) 3418–3419.
[17] B.L. Pierce, R. Ballard-Barbash, L. Bernstein, R.N. Baumgartner, M.L. Neuhouser, M.H. Wener, Elevated biomarkers of inflammation are associated with reduced survival among breast cancer patients, J. Clin. Oncol. 27 (2009) 3437–3444.
[18] M.G. Gamesan, N.D. Weiner, G.L. Flynn, N.F.H. Ho, Influence of liposomal drug entrapment on percutaneous absorption, Int. J.Pharm. 20 (1984) 139–154.
[19] D. Khossravi, Drug-surfactant interactions: effect on transport properties, Int. J. Pharm. 155 (1997) 179–190.
[20] J.-H.S. Kuo, M.-S. Jan, C.-H. Chang, H.-W. Chiu, C.-T. Li, Cytotoxicity characterization of catanionic vesicles in RAW 264.7 murine macrophage-like cells, Colloid Surf 41 (2005) 189–196.
[21] D. Liu, J. Hu, W. Qiao, Z. Li, S. Zhang, L. Cheng, Synthesis of carbamate-linked lipids for gene delivery, Bioorg. Med. Chem. Lett. 15 (2005) 3147–3150.
[22] D. Liu, W. Qiao, Z. Li, X. Cui, K. Li, L. Yu, K. Yan, L. Zhu, L. Cheng, Carbamate-linked cationic lipids for gene delivery, Bioorg. Med. Chem. 16 (2008) 995–1005.
[23] W. Qiao, M. Zhou, Hydroxyl-modified cationic lipids with a carbamate linkage as gene delivery vehicles, Eur. J. Lipid Sci. Technol. 115 (2013) 483–489.
[24] Z.D. Zhi, S. Zhang, F. Qureshi, Y. Zhao, S. Cui, B. Wang, H. Chen, B. Yang, D. Zhao, Structure- activity relationship of carbamate-linked cationic lipids bearing hydroxyethyl head group for gene delivery, Colloid Surf 112 (2013) 537–541.
[25] J. Shi, S.J. Yu, J. Zhu, D.F. Zhi, Y.N. Zhao, S.H. Cui, S.B. Zhang, Carbamate-linked cationic lipids with different hydrocarbon chains for gene delivery, Colloid Surf 141 (2016) 417–422.
[26] N.R. Kuznetsova, E.V. Stepanova, N.M. Peretolchina, D.A. Khochenkov, I.A. Boldyrev, N.V. Bovin, E.L. Vodovozova, Targeting liposomes loaded with melphalan prodrug to tumour vasculature via the Sialyl Lewis X selectin ligand, J. Drug Target. 22 (2014) 242–250.
[27] S. Han, T. Quach, L. Hu, A. Wahab, W.N. Charman, V.J. Stella, N.L. Trevaskis, J.S. Simpson, C.J. Porter, Targeted delivery of a model immunomodulator to the lymphatic system: comparison of alkyl ester versus triglyceride mimetic lipid prodrug strategies, J. Control. Release 177 (2014) 1–10.
[28] S. Zalipsky, M. Saad, R. Kiwan, E. Ber, N. Yu, T. Minko, Antitumor activity of new liposomal prodrug of mitomycinC in multidrug resistant solid tumor: insights of the mechanism of action, J. Drug Target. 15 (2007) 518–530.
[29] A.A. Gabizon, D. Tzemach, A.T. Horowitz, H. Shmeeda, J. Yeh, S. Zalipsky, Reduced toxicity and superior therapeutic activity of a mitomycinC lipid-based prodrug incorporated in pegylated liposomes, Clin. Cancer Res. 12 (2006) 1913–1920.
[30] L. Hu, T. Quach, S. Han, S.F. Lim, P. Yadav, D. Senyschyn, N.L. Trevaskis, J.S. Simpson, C.J.H. Porter, Glyceride-mimetic prodrugs incorporating self-immolative spacers promote lymphatic transport, avoid first-pass metabolism, and enhance oral bioavailability, Angew. Chem. Int. Edit. 55 (2016) 13700–13705.
[31] L. Zhang, Y.K. Feng, H. Tian, M. Zhao, M. Khan, J.T. Guo, Amphiphilic depsipeptide-based block copolymers as nanocarriers for controlled release of ibuprofen with doxorubicin, J. Polym. Sci. Pol. Chem. 51 (2013) 3213–3226.
[32] V.C. Sekera, C.S. Marvel, Higher alkyl sulfonates, J. Am. Chem. Soc. 55 (1933) 345–349.
[33] P.L. Felgner, T.R. Gadek, M. Holm, R. Roman, H.W. Chan, M. Wenz, J.P. Northrop, G.M. Ringold, M. Danielsen, Lipofection: a highly efficient, lipid-mediated DNA-transfection procedure, Proc. Natl. Acad. Sci. U. S. A. 84 (1987) 7413–7417.
[34] A. Ridell, H. Evertsson, S. Nilsson, L.O. Sundeloef, Amphiphilic association of ibuprofen and two nonionic cellulose derivatives in aqueous solution, J. Pharm. Sci. 88 (1999) 1175–1181.
[35] D. Kumar, M.A. Rub, N. Azum, A.M. Asiri, Mixed Micellization study of ibuprofen (sodium salt) and cationic surfactant (conventional as well as gemini), J. Phys. Org. Chem. 31 (2018) 3730.
[36] T. Asakawa, K. Ishikawa, K. Miyagishi, Aqueous solution properties of pyridinium-type perfluorinated surfactants and simulation of mixture CMC, J. Colloid. Interf. Sci. 240 (2001) 365–367.
[37] R. Sanan, R. Kaur, R.K. Mahajan, Micellar transitions in catanionic ionic liquid–ibuprofen aqueous mixtures; effects of composition and dilution, RSC Adv. 4 (2014) 64877–64889.
[38] K.L. Mittal, Solution chemistry of surfactants, J. Electrochem. Soc. 127 (1980) 337–354.
[39] P.M. Holland, Modeling Mixed Surfactant Systems, 1992 31–44.
[40] M.J. Rosen, Molecular interaction and the quantitative prediction of synergism in the mixtures of surfactants, Colloid Polym. Sci. 109 (1998) 35–41.
[41] D. Das, K. Ismail, Aggregation and adsorption properties of sodium dodecyl sulfate in water-acetamide mixtures, J. Colloid Interf. Sci. 327 (2008) 198–203.
[42] O.G. Singh, K. Ismail, Micellization behavior of mixtures of sodium dioctylsulfosuccinate with sodium dodecylsulfate in water, J. Surfact.Deterg. 11 (2008) 89–96.
[43] M.J. Rosen, X.Y. Hua, Surface concentrations and molecular interactions in binary mixtures of surfactants, J. Colloid Interf. Sci. 86 (1982) 164–172.
[44] S. Ghosh, S.P. Moulik, Interfacial and micellization behaviors of binary and ternary mixtures of amphiphiles (tween-20, Brij-35, and sodium dodecylsulfate) in aqueous medium, J. Colloid Interf. Sci. 208 (1998) 357–366.
[45] I. Mukherjee, S.P. Moulik, A.K. Rakshit, Tensiometric determination of gibbs surface excess and micelle point: a critical revisit, J. Colloid Interf. Sci. 394 (2013) 329–336.
[46] A. Srivastava, K. Ismail, Binding of phenol red to cetylpyridinium chloride at air solution and micelle–solution interfaces in aqueous ethylene glycol media, Colloid. Surface. A. 462 (2014) 115–123.
[47] A. Srivastava, C. Liu, H. Fang, J. Lv, W. Qiao, Interaction and binding efficiency of cationic drug chlorpheniramine maleate — anionic amino acid gemini surfactants mixture as media for the Synthesis of silver nanoparticles, Colloid. Surface. A. 529 (2017) 686–695.
[48] L. Jin, D.Y. Choi, H. Liu, K.H. Row, Protein binding study of S-ibuprofen using high-performance frontal analysis, B. Korean Chem. Soc. 26 (2005) 136–138.
[49] T.G. Burke, T.R. Tritton, Structural basis of anthracycline selectivity for unilamellar phosphatidylcoline vesicles: an equilibrium binding study, Biochemistry 24 (1985) 1768–1776.
[50] D. Agudelo, P. Bourassa, J. Bruneau, G. Be'rube´, E. Asselin, H. A. Tajmir-Riahi. Probing the binding sites of antibiotic drugs doxorubicin and N- (trifluoroacetyl) doxorubicin with human and bovine serum albumins.PlosOne 2012, 7, 43814.
[51] U. Kragh-Hansen, Structure and ligand binding properties of human serum albumin, Dan. Med. Bull. 37 (1990) 57–84.
[52] N.A. Kratochwil, W. Huber, F. Muller, M. Kansy, P.R. Gerber, Predicting plasma protein binding of drugs: a new approach, Biochem. Pharmacol. 64 (2002) 1355–1374.
[53] Y. Bai, X.D. Fan, H. Yao, Z. Yang, T.T. Liu, H.T. Zhang, W.B. Zhang, W. Tian, Probing into the supramolecular driving force of an amphiphilic B-cyclodextrin dimer in various solvents: host—guest recognition or hydrophilic—hydrophobic interaction, J. Phys. Chem. B 119 (2015) 11893–11899.
[54] S. Segota, S. Heimer, D. Tezak, New catanionic mixtures of dodecyldimethyl ammonium bromide/sodium dodecylbenzenesulphonate/water I, surface properties of dispersed particles, Colloids Surf. A Physicochem. Eng. Asp. 274 (2006) 91–99.
[55] F. Li, Y. Luan, X. Liu, G. Xu, X. Li, J. Wang, Investigation on the aggregation behaviors of DDAB/NaDEHP catanionic vesicles inthe absence and presence of a negatively charged polyelectrolyte, Phys. Chem. Chem. Phys. 13 (2011) 5897–5905.

[56] A. Srivastava, C. Liu, J. Lv, D.K. Deb, W. Qiao, Enhanced intercellular release of anticancer drug by using Nano-sized catanionic vesicles of doxorubicin hydrochloride and gemini surfactants, J. Mol. Liqs. 259 (2018) 398–410.
[57] J. Fang, H. Nakamura, H. Maeda, The EPR effect: unique features of tumor blood vessels for drug delivery, factors involved, and limitations and augmentation of the effect, Adv. Drug Deliver. Rev. 63 (2011) 136–151.
[58] N. Bertrand, J. Wu, X. Xu, N. Kamaly, O.C. Farokhzad, Cancer nanotechnology: the impact of passive and active targeting in the era of modern cancer biology, Adv. Drug Deliver. Rev. 66 (2014) 2–25.
[59] E. Blanco, H. Shen, M. Ferrari, Principles of nanoparticle design for overcoming biological barriers to drug delivery, Nat. Biotechnol. 33 (2015) 941–951.